Central European Journal of Energetic Materials
ISSN 1733-7178; e-ISSN 2353-1843

Cent. Eur. J. Energ. Mater. 2024, *21*(2): 210-229; DOI 10.22211/cejem/190547
Article is available in PDF-format, in colour, at:
https://ipo.lukasiewicz.gov.pl/wydawnictwa/cejem-woluminy/vol-21-nr-2/

Research paper

Oxidant-Accelerated Polymerization of Dopamine for Coating DNAN with Enhanced Toughness

Jinshan Li*), Chun Xiao, Guoqiang Liu, Shuyi Duan, Baohui Zheng, Qing Zhu
Institute of Chemical Materials, China Academy of Engineering Physics, China
* *E-mail:* ljs915@263.net

Abstract: Due to the significantly reduced toxicity and shock sensitivity compared to TNT, DNAN is getting more and more attention in the study of insensitive munitions. However, the brittleness problem of DNAN limits its wide application. Inspired by mussels, DNAN particles with a thin and uniform coating based on the self-polymerization of dopamine were prepared by an oxidant-accelerated method in this work. XRD patterns indicated that the DNAN polymorph did not change during the coating process. FT-IR and XPS spectra manifested that the PDA was successfully distributed on the crystal surface. The results of TG-DSC analysis demonstrated that the mass ratio of PDA coating was as low as 1.71%. Meanwhile, Brazilian disk splitting test showed that the tensile strength, tensile strain, and fracture energy of DNAN@PDA cylinder were 16.1%, 32.0% and 53.0% higher than those of pure DNAN cylinder, respectively. The morphology of fracture surface after tensile test indicated that toughness fracture occurred in DNAN@PDA cylinder, while remarkable brittle fracture occurred in pure DNAN cylinder. The surface modification method could enhance the toughness of DNAN-based explosives, and the fast fabrication of DNAN@PDA particles on a large scale could satisfy the application demands of insensitive munitions.

Keywords: insensitive munitions, 2,4-dinitroanisole, DNAN, polydopamine, toughness fracture, mechanical properties

1 Introduction

Security accidents happened during use, storage and transportation of munitions will cause huge casualties and property losses, so the demand for insensitive munitions (IM) is more and more urgent [1-3]. Compared with 2,4,6-trinitrotoluene (TNT), 2,4-dinitroanisole (DNAN) has significantly reduced toxicity and sensitivity to shock and impact [4-8], and is an important insensitive energetic compound [9, 10]. Currently, DNAN has been applied in the insensitive explosive formulations such as IMX-101, IMX-104 and PAX-21 [11-13].

However, the brittleness problem of traditional melt-cast explosive still exists in DNAN [14]. When the explosive charge with poor toughness is subjected to friction and shear stress caused by strong overload, it is easy to generate damage and micro-cracks, thus forming hot spots and reducing the safety of ammunitions [15, 16]. Therefore, it is of great significance to improve the toughness of DNAN to promote its application.

It is a conventional method to improve the toughness by coating energetic crystals with appropriate amount of polymer [17, 18], but the coverage of energetic crystal is usually low, and interfacial interactions between polymer and energetic crystal are unsatisfactory. Recently, in situ polymerization method has attracted considerable interests in the field of surface modification for explosive crystals [19, 20]. Although in situ polymerization technique could improve the coverage to a certain extent, the weaker van der Waals interactions between explosive crystal and polymer could not significantly improve the toughness. Therefore, it is essential to develop a new strategy to modify energetic crystals with novel strong adhesion materials.

Inspired by the super adhesion of mussels, polydopamine (PDA) has been demonstrated to construct thin, uniform, full-covered coating layer on the surface of energetic particles [21-23]. The PDA coating layer enhances the interfacial interactions between energetic crystal and binder because of its diverse active groups such as –OH and $–NH_2$ [24]. In our previous work, surface modification of HMX, TATB and aluminum powder was carried out by self-polymerization of dopamine, indicated that a PDA surface layer could reduce the mechanical sensitivity of HMX [25], enhance the tensile strength of TATB-based PBX cylinder [26], and slow down the sedimentation of aluminum powder in HTPB liquid phase [27]. What's more, we developed an oxidant-accelerated method to obtain fast PDA surface modification of HMX particles within 5 min [28], showing a capability to fabricate HMX@PDA particles on a large scale. Until now, a lot of works have been studied on the research about energetic materials coated with PDA, such as RDX, CL-20, LLM-105 and 2,6-diamino-

3,5-dinitropyrazine-1-oxide (ANPZO) [29-31]. Therefore, it is reasonable to speculate that the advantages of PDA coating may provide an alternative method for reducing the brittleness of DNAN.

Herein, we demonstrate a simple and quick method to prepare interfacial enhanced DNAN@PDA particles based on the oxidant-accelerated self-polymerization process of dopamine. The surface of DNAN particles was homogeneously covered by the formed PDA coating. The prepared particles showed stable physical properties, though the PDA coating was very thin. The DNAN@PDA cylinder manifested higher tensile strength and remarkable feature of toughness fracture. The findings in this study offer a facile and alternative method for the large scale manufacture of toughened DNAN particles.

2 Experimental Sections

2.1 Materials

DNAN was produced by Dongfang Chemical Industry Group Co., Ltd. Tested DNAN has a melting point of 94-96 °C and a density of 1.52 g/cm^3, with a purity of 99.6 ±0.3%. Dopamine hydrochloride (DA), sodium periodate ($NaIO_4$) and 2-amino-2-hydroxymethylpropane-1,3-diol (Tris) were provided by Aladdin Chemical Ltd. All reagents were used as-received without further purification.

2.2 Preparation of the DNAN@PDA particles

The original DNAN particles were washed with deionized water and ethanol for several times and dried at 50 °C before use. The reaction solution consisted of DA (8 mmol) and Tris (40 mmol) dissolved in deionized water (200 mL). And then $NaIO_4$ (16 mmol) was added as an oxidant. To this solution, DNAN (10 g) was added and stirred for 5 min using stirrer paddle with 100 rpm to produce DNAN@PDA particles [28]. The resultant particles were washed with 50 mL deionized water three times and dried at 50 °C for 6 h for further characterizations.

2.3 Characterizations

The morphologies of pristine DNAN particles and PDA modified DNAN particles were observed by a scanning electron microscope (CamScan Apollo 300). The samples were randomly selected and taped to the sample table with conductive tape, then sputter coated with gold for 40 s at a current of 20 mA for further analysis.

Fourier transform infrared spectrometer (FT-IR) spectra were carried out on a BRUKER VERTEX70 instrument by transmission method from 500 to

4000 cm^{-1}, 32 scans were accumulated in all cases, with a spectral resolution of 4 cm^{-1}. DNAN and DNAN@PDA particles were mixed with KBr powders, and then pressed at 10 MPa for 3-5 min.

X-ray photoelectron spectroscope (XPS) spectra were performed on a Thermo ESCACAB250 instrument. TG-DSC measurements were recorded with a NETZSCH STA 448 C instrument from room temperature to 500 °C (heating rate of 10 °C/min and N_2 atmosphere). X-ray diffraction (XRD) patterns were collected on a BRUKER D8 instrument using Cu Kα source.

The pristine DNAN and DNAN@PDA powders were cold-pressed into cylinder in size of *Φ*20×6 and *Φ*20×20 mm for Brazilian test and compression test. The molding specific pressure was 180 MPa and the holding time was 30 min. The Brazilian disk splitting test and compression test were performed on an explosion-proof modified universal testing machine. Both tests used a rate of 0.5 mm/min, and curved platens were used in Brazilian test.

3 Results and Discussion

3.1 Morphologies of pristine DNAN and as-prepared DNAN@PDA particles

After being stirred in dopamine-$NaIO_4$-Tris buffer solution, the as-prepared DNAN@PDA particles displayed a dark brown appearance due to the formation of a PDA coating on the DNAN surface. The median particle diameters (d_{50}) of DNAN and DNAN@PDA are 376.6 and 347.9 μm, respectively. The morphologies of the DNAN particles before and after coating were observed by SEM measurements (Figure 1), showing that the shapes of DNAN and DNAN@PDA particles have no change. After reaction, the surface of DNAN particles was obviously covered with a coating film.

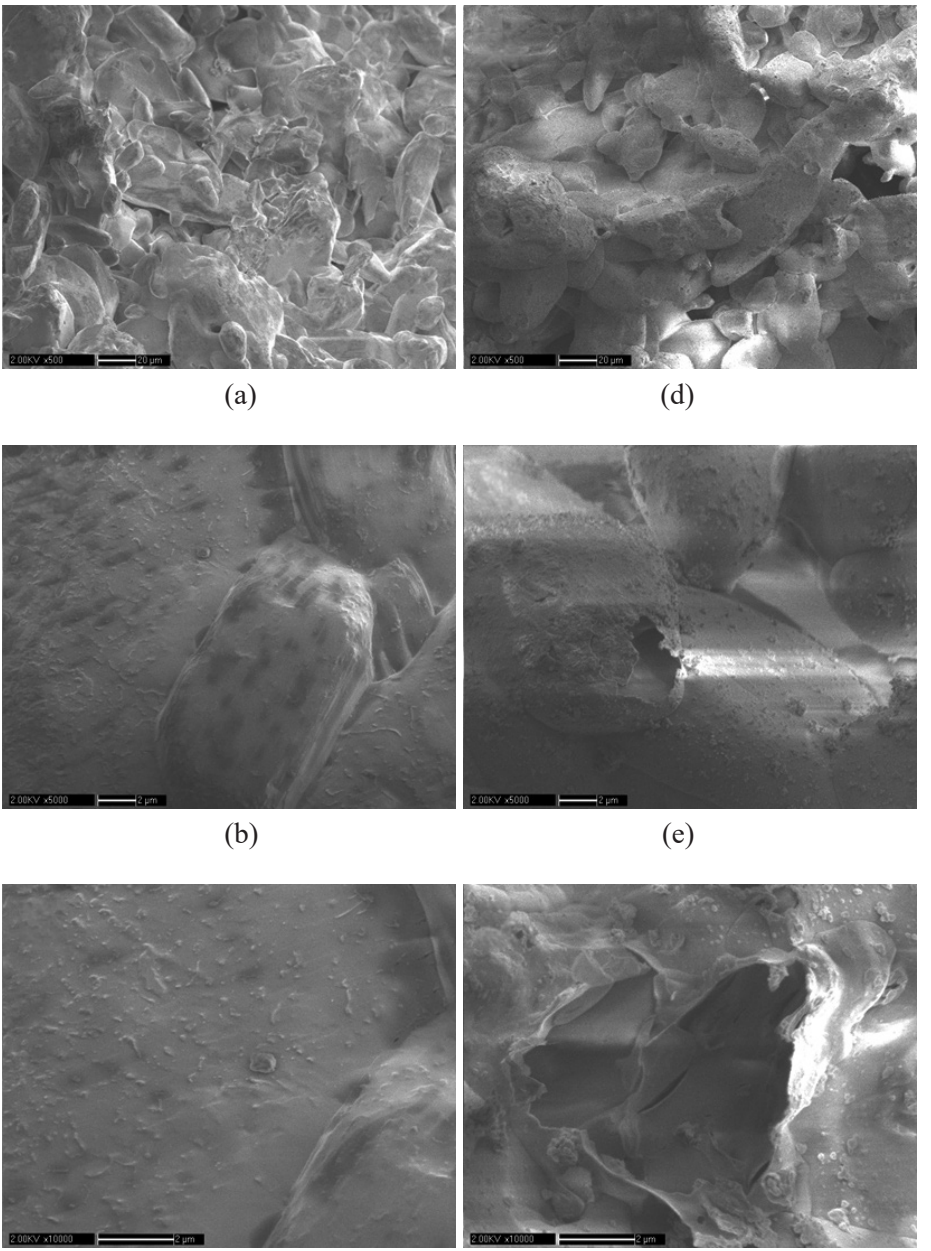

Figure 1. SEM images of the DNAN (a-c) and DNAN@PDA (d-f) particles

3.2 Structures of pristine DNAN and as-prepared DNAN@PDA particles

XRD patterns of the DNAN and DNAN@PDA particles confirmed that the 2θ values of 14.01°, 15.97°, 18.79°, 22.41°, 24.86° and 26.23° were consistent with DNAN-I type [32] for both in the region of 10-50° (Figure 2). The results of the XRD patterns indicated that the PDA coating did not change the polymorph of DNAN particles.

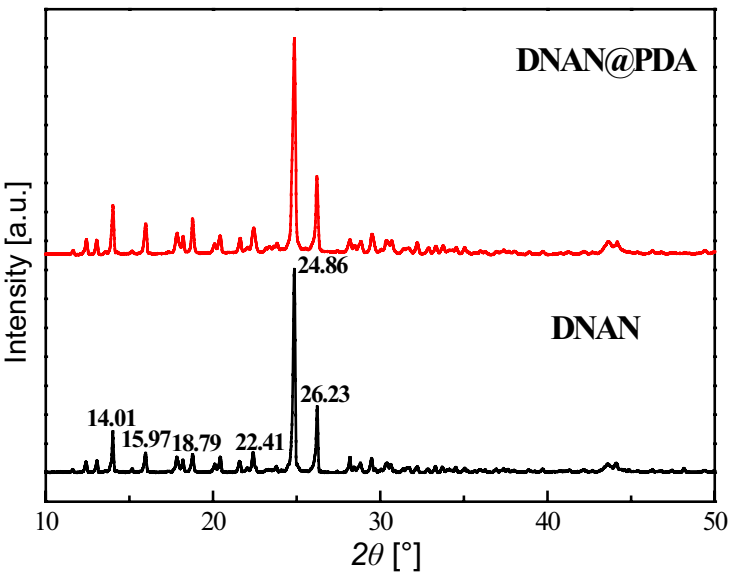

Figure 2. XRD patterns of the DNAN and DNAN@PDA particles

TG-DSC measurements showed decomposition processes of the samples at increasing temperatures. But in an open crucible, DNAN would evaporate before it decomposes, and then dissipate with the gas flow (Figure 3). The mass losses for the DNAN and DNAN@PDA before 500 °C were 100% and 98.99%, respectively. The PDA polymer was also measured by TG/DSC method under the same condition as DNAN@PDA, and the results were showed in Figure 4. PDA began to decompose slowly from about 250 °C, and the weight loss was 41.1% when the temperature rose to 500 °C. Taking into account the decomposition of PDA itself, the content of PDA coating was approximately 1.71%. In order to study the effect of PDA coating on thermal decomposition performance of DNAN, a sealed crucible was used in the DSC test, and the results were showed in Figure 5. It manifested that PDA coating had no effect on the melting temperature of DNAN, and the peak decomposition temperature of DNAN@PDA was reduced

by 23.4 °C. But the onset decomposition temperature of DNAN@PDA is over 250 °C, and the peak decomposition temperature reaches 328.2 °C, showing that DNAN@PDA has good thermal stability.

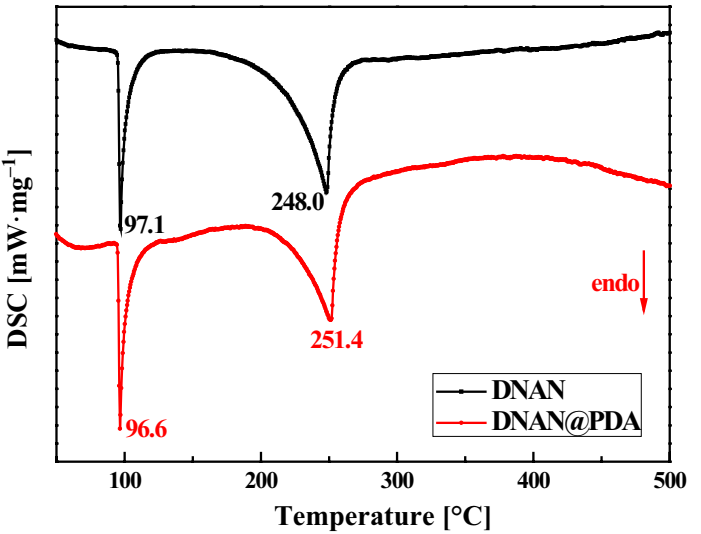

(a)

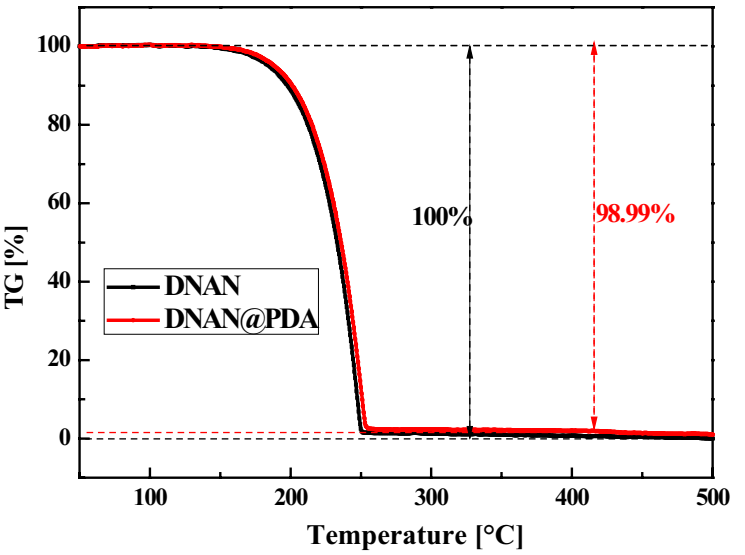

(b)

Figure 3. DSC (a) and TG (b) results of pristine DNAN and DNAN@PDA (in open crucible)

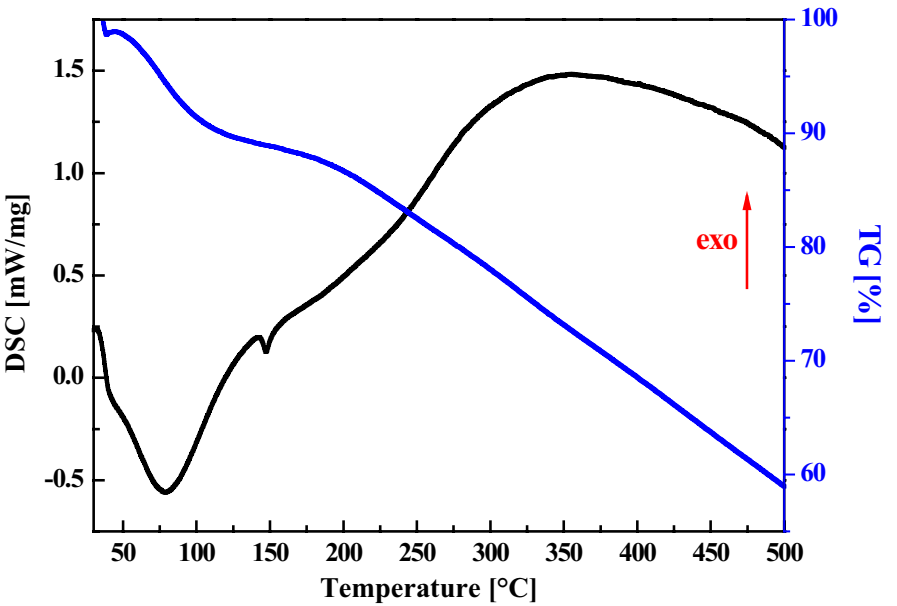

Figure 4. DSC-TG results of PDA (in open crucible)

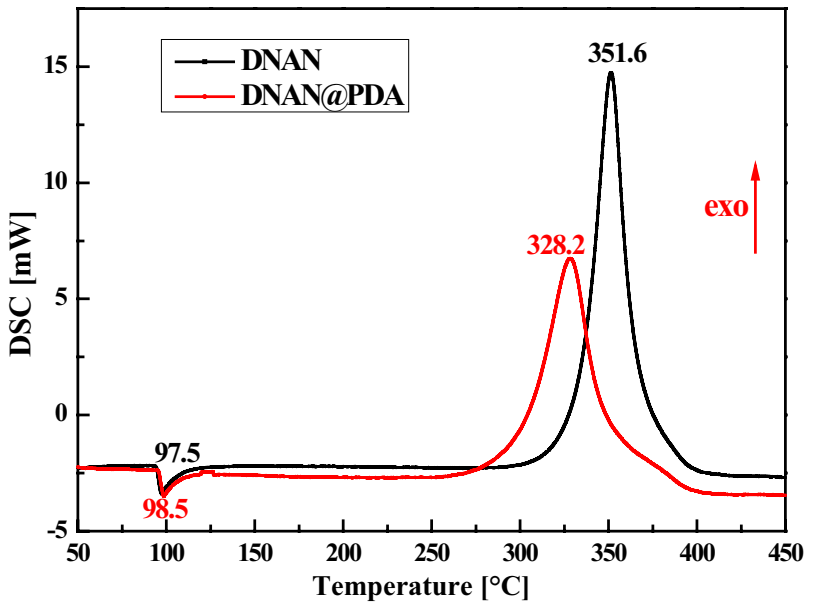

Figure 5. DSC results of pristine DNAN and DNAN@PDA (in sealed crucible)

3.3 Surface characteristics of pristine DNAN and as-prepared DNAN@PDA particles

The presence of the PDA coating on the surface of the DNAN particles was demonstrated by FT-IR and XPS spectra of the DNAN and DNAN@PDA particles. As shown in Figure 6, the peaks at 1522 and 1342 cm^{-1} are attributed to the stretching vibration of nitrobenzene. The absorption bands at 745, 835 and 1605 cm^{-1} are ascribed to the bending vibrations of C–N, C–N–O, and benzene skeleton vibration, whereas absorption bands at 1072 and 1282 cm^{-1} belong to the symmetrical and anti-symmetric stretching vibration of phenyl ether. The peak at 3090 cm^{-1} is attributed to the stretching vibration of aromatic hydrocarbon. The peak at 921 cm^{-1} belongs to the out-plane bending vibration of aromatic hydrocarbon, whereas absorption bands at 1072 and 1282 cm^{-1} are both ascribed to its in-plane bending vibration. The main difference of functional group between PDA coating and DNAN is N–H group, whose absorption peak coincides with nitrobenzene in DNAN, so the characteristic peaks of DNAN@PDA are basically consistent with that of DNAN.

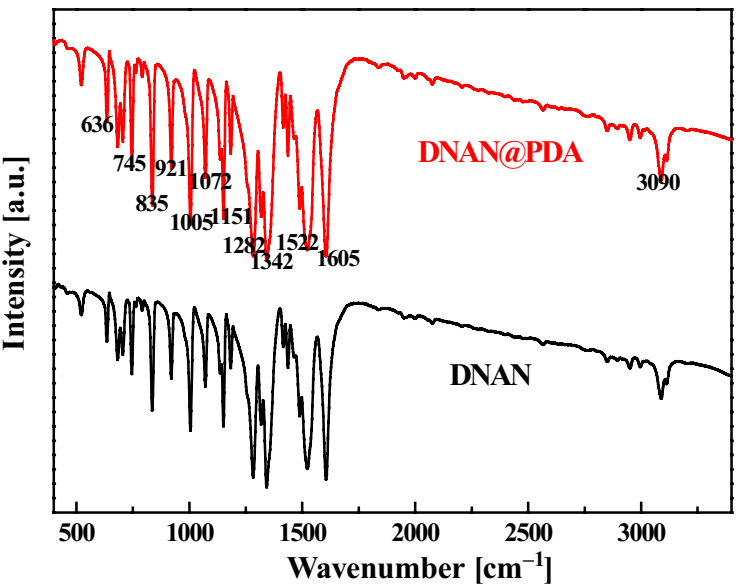

Figure 6. FT-IR spectra of the DNAN and DNAN@PDA particles

The changes as a result of the coating on the DNAN particles were further confirmed by XPS. Table 1 showed the comparison of the element content of the particle surface. The average carbon atom content on the DNAN surface increased

from 55.26% to 64.96% and the average contents of oxygen and nitrogen atoms decreased after modification because of the high carbon atom content for PDA. Figures 7 and 8 showed the XPS spectra of DNAN and DNAN@PDA particles. Survey scans revealed the elements of C, N, and O on the surface of the particles. The C1s spectrum of DNAN showed typical components of C–C (284.1 eV), C–N (285.1 eV), and C–O (286.0 eV), which were also detected on the surface of DNAN@PDA particles. The extra component of C=O (288.0 eV) [33] was derived from the PDA coating. This deduction was also supported by the peaks at 530.4 and 533.1 eV in the O1s spectrum, corresponding to C=O and C–OH, respectively. The peaks at 532.4 eV of DNAN@PDA and 532.8 eV of DNAN were both corresponded to C–O. The peak at 531.8 eV in the O1s spectrum of DNAN was corresponded to N–O, which was also supported by the peak at 404.8 eV in the N1s spectrum. The N1s spectrum of DNAN@PDA could be divided into two components at 399.4 and 405.6 eV, corresponding to C–N and $–NH_2$, respectively [34]. The presence of C–OH, C=O and $–NH_2$ species suggested the PDA coating on the surface of DNAN particles after modification. These diverse active groups in the PDA coating could serve as anchors for further attachment and reaction, which could improve the adhesion between energetic particles in cylinder.

Table 1. Average element content of DNAN and DNAN@PDA particle surface

Samples	Average element content on the surface [%]		
	C	N	O
DNAN	55.26	12.93	31.81
DNAN@PDA	64.96	10.87	24.17

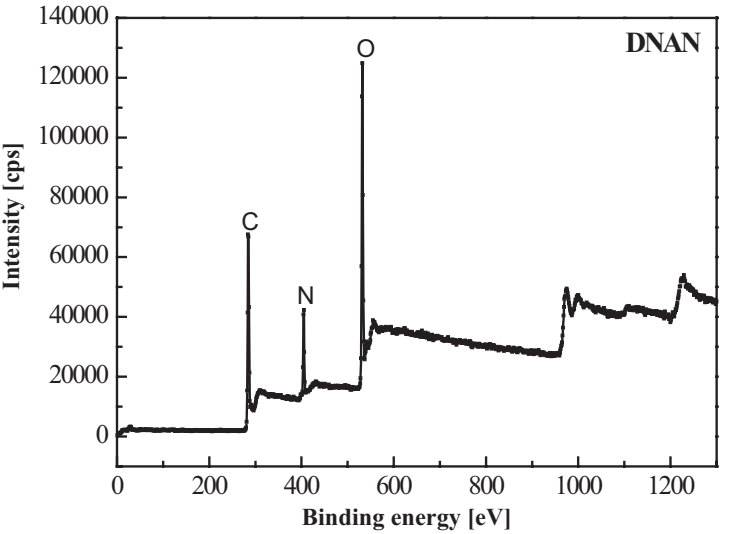

(a)

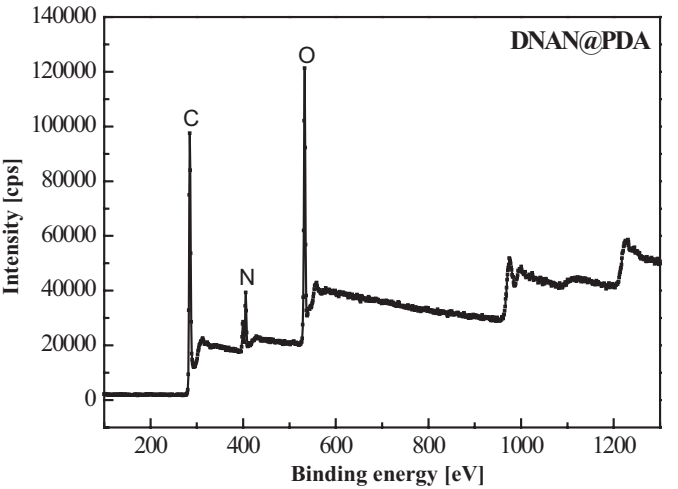

(b)

Figure 7. XPS spectra of DNAN (a) and DNAN@PDA (b) particles

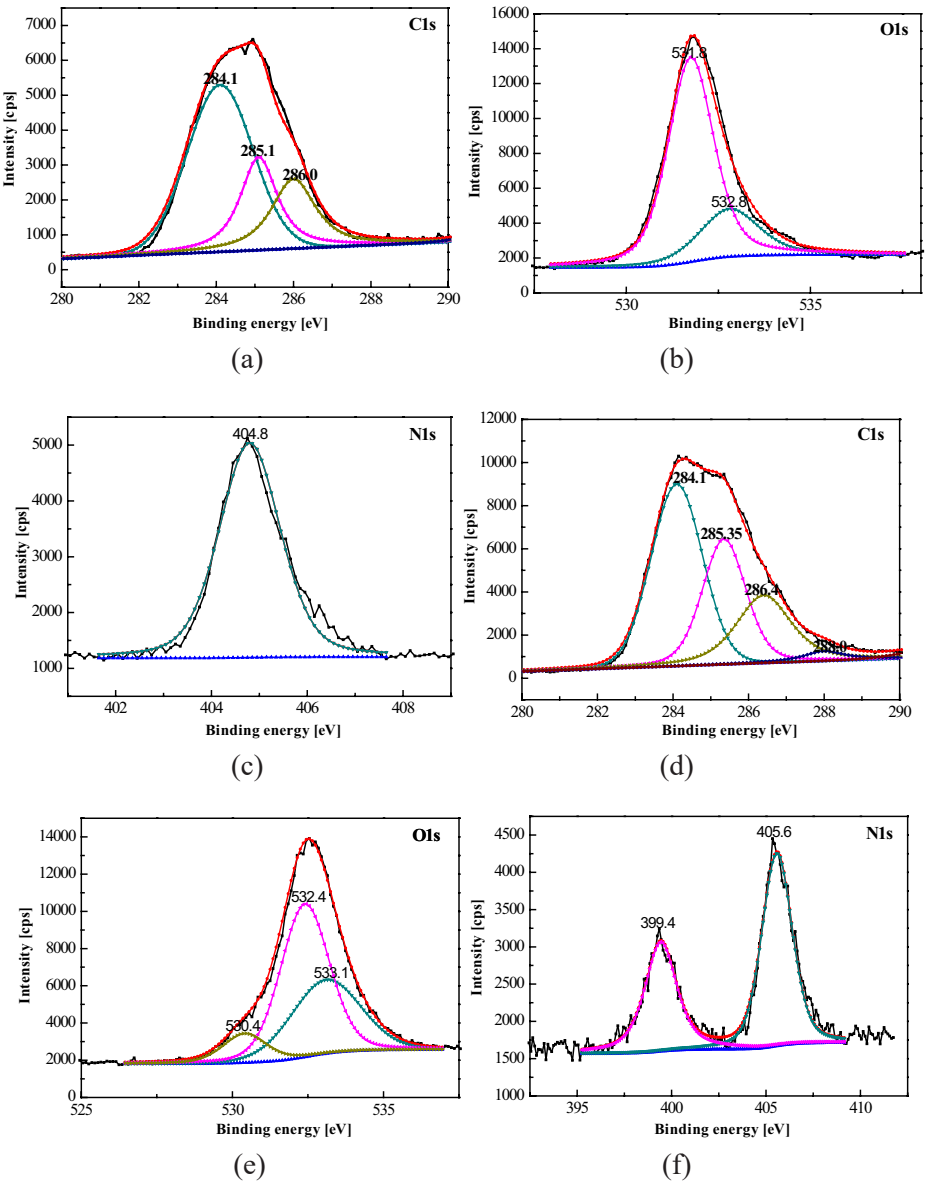

Figure 8. Survey scans on the surface of DNAN (a-c) and DNAN@PDA (d-f) particles

3.4 Mechanical properties of compressed DNAN and DNAN@PDA cylinder

In order to investigate the influence of PDA coating on mechanical properties of explosive, DNAN and DNAN@PDA cylinder were compressed, followed by the test of tensile and compressive properties. The actual density of the cylinder was 97.5% of the theoretical density. As shown in Table 2, the tensile strength of DNAN@PDA cylinder was enhanced by 16.1% and the tensile strain was improved by 32.0% compared to DNAN cylinder, while the tensile modulus was decreased for a little. As to the compressive property (Table 3), the compression strength and modulus of DNAN@PDA cylinder were both lower than DNAN cylinder, and the degree of reductions were 10.5% and 22.5%, respectively. But the compression strain increased by 16.6%.

Fracture energy refers to the energy required by the crack of specimen extend per unit area under tensile load, which is equal to the area contained under the load-displacement curve. The stress-strain curves showed in Figure 9 was converted into load-displacement curves using the following formulas.

$$F = \frac{\pi DH\sigma}{2} \tag{1}$$

$$s = \varepsilon \mathrm{D} \tag{2}$$

where F represents the load applied to the specimen (in N), D and H refer to the diameter and thickness of the specimen (in mm), represents the tensile strength of the specimen (in MPa), s refers to the displacement of the specimen (in mm) and ε refers to the strain of the specimen (in %).

The fracture energy of DNAN cylinder and DNAN@PDA cylinder were obtained by integrating the area under the load-displacement curves, which were 110.6 and 169.2 N/mm, respectively. The latter represented a 53.0% increase over the former. The compared results revealed a better tensile property of the cylinder prepared from DNAN@ PDA particles, implying the brittleness of the DNAN@PDA cylinder was weakened.

Table 2. Tensile properties of compressed DNAN and DNAN@PDA cylinder

Samples	Tensile strength [MPa]	Tensile strain [%]	Tensile modulus [GPa]
DNAN	2.05	0.025	5.52
DNAN@PDA	2.38	0.033	5.20

Table 3. Compression properties of compressed DNAN and DNAN@PDA cylinder

Samples	Compression strength [MPa]	Compression strain [%]	Compression modulus [GPa]
DNAN	38.15	0.697	6.53
DNAN@PDA	34.13	0.813	5.06

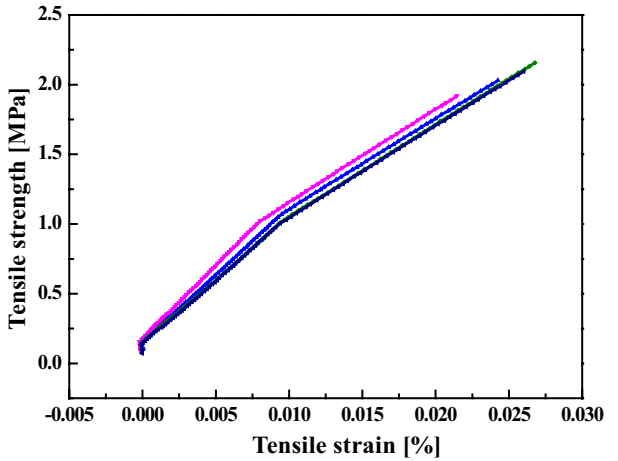

(a)

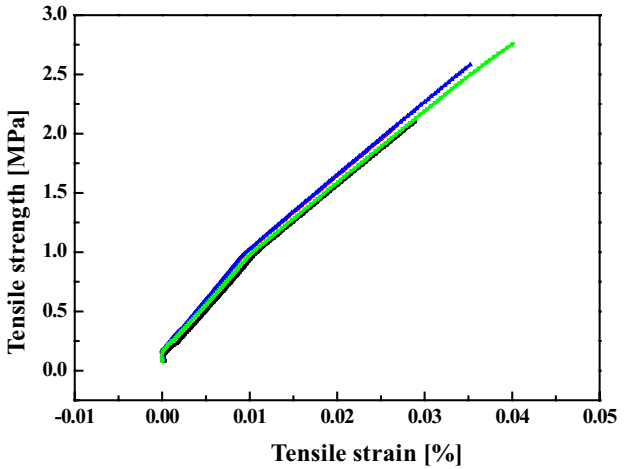

(b)

Figure 9. Tensile stress-strain curves of DNAN (a) and DNAN@PDA (b) cylinder

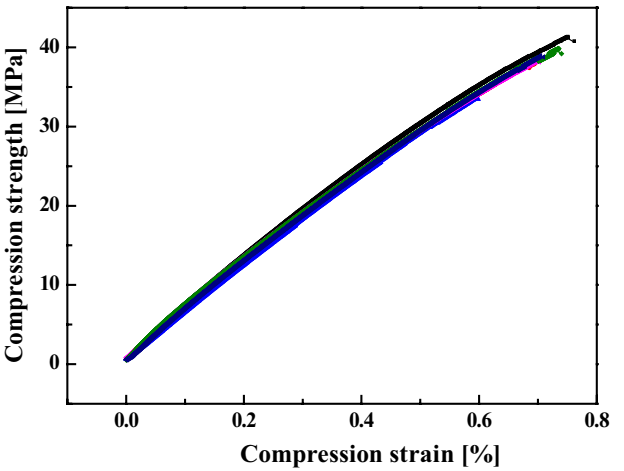

(a)

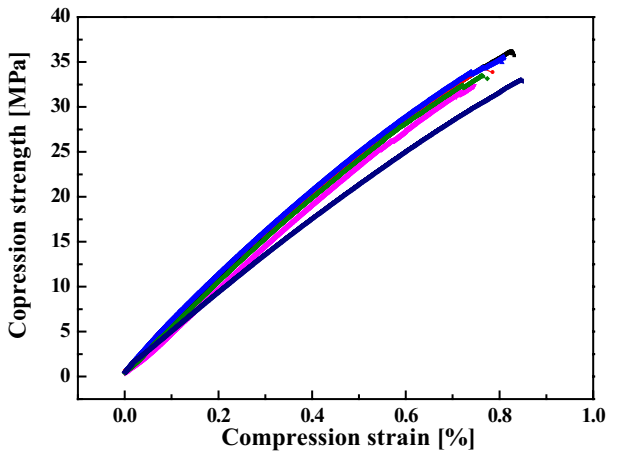

(b)

Figure 10. Compression stress-strain curves of DNAN (a) and DNAN@PDA (b) cylinder

Furthermore, the fracture surface of the cylinder after tensile test was observed by SEM, and the results was showed in Figure 11. Interestingly, the fracture surface of DNAN cylinder appeared stripe-type grooves, and the grooves had a relatively smooth surface, manifesting a brittle fracture. For the DNAN@PDA cylinder, the fracture surface was significantly rough. The interaction between DNAN crystal and PDA coating might enhance the toughness of the cylinder.

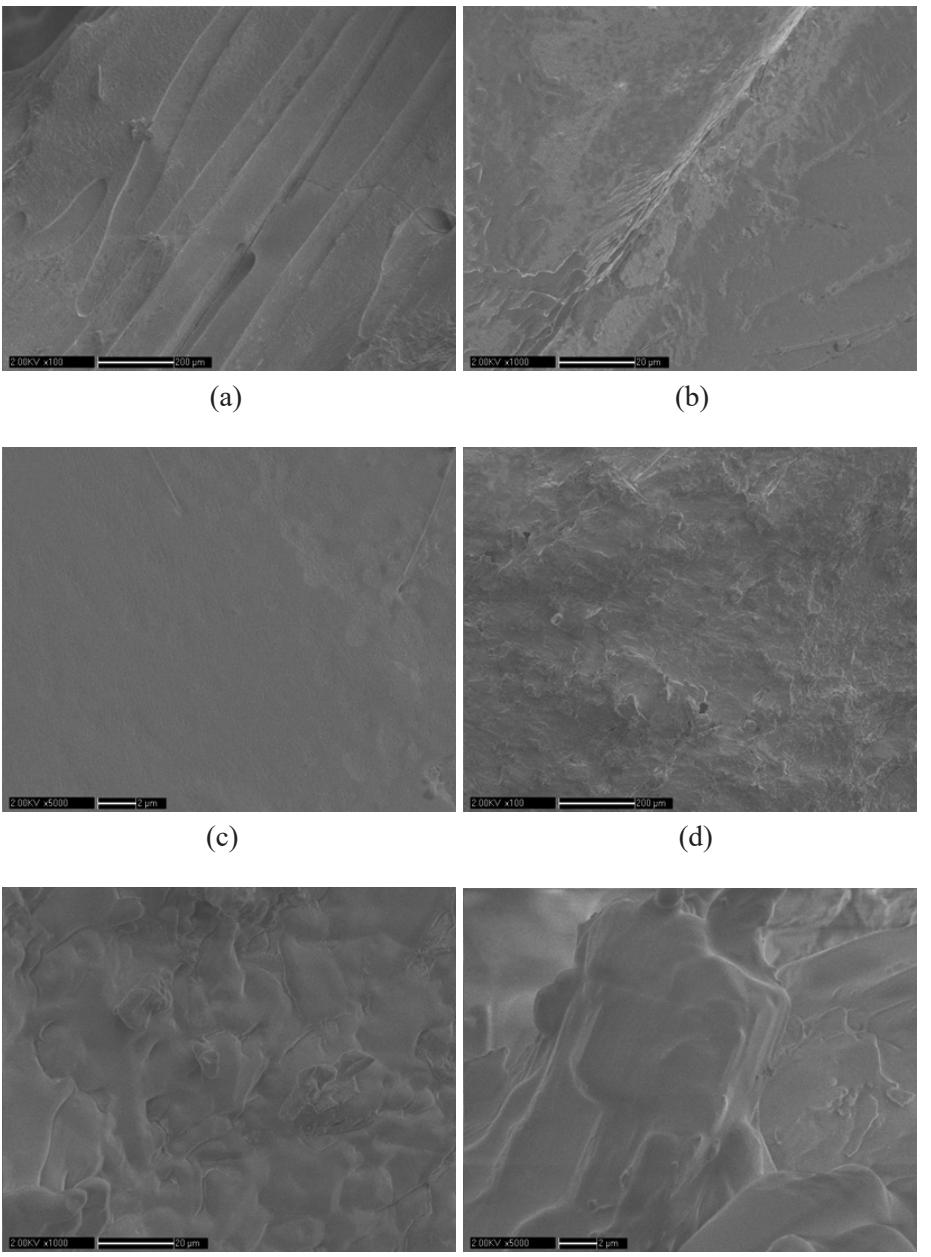

Figure 11. SEM images of the fracture surface of DNAN cylinder (a-c) and DNAN@PDA cylinder (d-f)

4 Conclusions

- In summary, this work demonstrated a facile one-step method for modifying the energetic material DNAN by applying a thin PDA coating. Upon the addition of $NaIO_4$ as oxidant, PDA coating layer was formed onto the surface of DNAN crystals within 5 min.
- The PDA coating on the surface of DNAN particles was thin and its mass proportion was slight, and the polymorph of DNAN crystals did not change during the coating process.
- The uniform PDA coating could improve the adhesive property between particles, which was reflected in the improvement of tensile property of DNAN@PDA cylinder. The fracture surface morphologies of the two samples also supported this view.

Acknowledgments

The authors are very grateful for the financial support from the National Natural Science Foundation of China (grant no. 22005281).

References

[1] Meng, J. J.; Zhou, L.; Miao, F. C. Review of the Essential Characteristics of 2,4-Dinitroanisole. *Cent. Eur. J. Energ. Mater.* **2023**, *20*(*1*): 50-74; https://doi.org/10.22211/cejem/1 62865.

[2] Osmar, M.; Warren, M. K.; Savia, G.; Reyes, S.; Eugene, A. M.; Leif, A.; Jim, A.F. Covalent Binding with Model Quinone Compounds Unveils the Environmental Fate of the Insensitive Munitions Reduced Product 2,4-Diaminoanisole (DAAN) Under Anoxic Conditions. *J. Hazard. Mater.* **2021**, *413*: paper 125459; https://doi.org/10.1016/j.jhazmat.2021.125459.

[3] Viktor, P.; Warren, K.; Samuel, B.; Hayden, M.; Edward, H.; Favianna, C.; Stephen, M.M.; Katerina, D. Transport of Insensitive Munitions Constituents, NTO, DNAN, RDX, and HMX in Runoff and Sediment Under Simulated Rainfall. *Sci. Total Environ.* **2023**, *866*: paper 161434; https://doi.org/10.1016/j.scitotenv.2023.161434.

[4] Sabine, G.D.; Manon, S.; Jalal, H.; Louise, P.; Guy, A.; Sonia, T.; Geoffrey, I.S. Ecotoxicological Assessment of a High Energetic and Insensitive Munitions Compound: 2,4-Dinitroanisole (DNAN). *J. Hazard. Mater.* **2013**, *262*: 143-150; https://doi.org/10.1016/j.jhazmat.2013.08.043.

[5] Trzciński, W.; Cudziło, S.; Dyjak, S.; Nita, M. A Comparison of the Sensitivity and Performance Characteristics of Melt-pour Explosives with TNT and DNAN Binder. *Cent. Eur. J. Energ. Mater.* **2014**, *11* (3): 443-455; https://doi.org/10.1109/JLT.2014.2342251.

[6] Yang, Y.; Duan, Z.P.; Li, S.R.; Han, Y.; Huang, H.; Zhang, L.S.; Huang, F.L. Detonation Characteristics of an Aluminized DNAN-Based Melt-Cast Explosive. *Propellants Explos. Pyrotech.***2023**, *48*: paper e202200088; https://doi.org/10.1002/prep.202200088.

[7] Eric, J.B.; Paul, G.T.; Tifany, L.T.; Kyle, C.E.; David, A.D.; Joseph, J.P.; Xu, W.Q. Computational Predictions of the Hydrolysis of 2,4,6-Trinitrotoluene (TNT) and 2,4-Dinitroanisole (DNAN). *J. Phys. Chem. A*. **2022**, *126*: 9059-9075; https://doi.org/10.1021/acs.jpca.2c06014.

[8] Manoj, K.S. Computational Prediction of Electronic Excited-State Structures and Properties of 2,4-Dinitroanisole (DNAN). *Struct. Chem.* **2016**, *27*: 1143-1148; https://doi.org/10.1007/s11224-015-0736-z.

[9] Shi, D.N.; Chen, L.Z.; Wang, J.L.; Chen, J.; Pan, H.X. Thermal Properties Study of Low-Melting-Point-DNAN and Analysis of Solidification Behavior of High-Melting-Point-DNAN. *Propellants Explos. Pyrotech.* **2021**, *46*: 1415-1420; https://doi.org/10.1002/prep.202100091.

[10] Zhu, D.L.; Zhou, L.; Zhang, X.R. Rheological Behavior of DNAN/HMX Melt-Cast Explosives. *Propellants Explos. Pyrotech.* **2019**, *44*: 1583-1589; https://doi.org/10.1002/prep.201900117.

[11] Nathan, S.; Aditi, P.; Ramesh, G. Biodegradation of Insensitive Munition (IM) Formulations: IMX-101 and IMX-104 Using Aerobic Granule Technology. *J. Hazard. Mater.* **2023**, *449*: paper 130942; https://doi.org/10.1016/j.jhazmat.2023.130942.

[12] Benjamin, K.; Stephen, M.M.; Li, L.; Viktor, P.; Warren, K.; Samuel, B.; Katerina, D. A Laboratory Rill Study of IMX-104 Transport in Overland Flow. *Chemosphere* **2023**, *310*: paper 136866; https://doi.org/10.1016/j.chemosphere.2022.136866.

[13] Michael, R.W.; Marianne, E.W.; Susan, T.; Charles, A.R.; David, B.R.; Jan, E.Z.; Sonia, T.; Guy, A.; Diaz, E. Characterization of PAX-21 Insensitive Munition Detonation Residues. *Propellants Explos. Pyrotech.* **2013**, *38*: 399-409; https://doi.org/10.1002/prep.201200150.

[14] Zhu, D.L.; Zhou, L.; Zhang, X.R.; Zhao, J.Y. Simultaneous Determination of Multiple Mechanical Parameters for a DNAN/HMX Melt-Cast Explosive by Brazilian Disc Test Combined with Digital Image Correlation Method. *Propellants Explos. Pyrotech.* **2017**, *42*: 864-872; https://doi.org/10.1002/prep.201700010.

[15] Li, S.R.; Duan, Z.P.; Gao, T.Y.; Wang, X.J.; Ou, Z.C.; Huang, F.L. Size Effect of Explosive Particle on Shock Initiation of Aluminized 2,4-Dinitroanisole (DNAN)-based Melt-cast Explosive. *J. Appl. Phys.* **2020**, *128*: paper 125903; https://doi.org/10.1063/5.0016310.

[16] Daniel, W.W.; Paul, L.C.; Colin, R.P. Preventing Irreversible Growth of DNAN by Controlling Its Polymorphism. *Proc. New Trends Res. Energ. Mater.*, Pardubice, Czech Republic, **2017**.

[17] Ma, Q.; Shu, Y.J.; Luo, G.; Chen, L.; Zheng, B.H.; Li, H.R. Toughening and Elasticizing Route of TNT Based Melt Cast Explosives. *Chin. J. Energet. Mater.* **2012**, *20*: 618-629; https://doi.org/10.3969 /j.issn.006-9941.2012.05.022.

[18] Meng, J.J.; Jiang, Z.M.; Zhang, X.R.; Zhou, L. Effect of Functional Agents on the Performance of 2,4-Dinitroanisole-based Melt-cast Explosives. *Acta Armamentarii* **2016**, *37*: 424-430; https://doi.org/10.3969 /j.issn.1000-1093.2016.03.006.
[19] Yang, Z.J.; Ding, L.; Wu, P.; Liu, Y.; Nie, F.D.; Huang, F.L. Fabrication of RDX, HMX and CL-20 Based Microcapsules *via In Situ* Polymerization of Melamine-Formaldehyde Resins with Reduced Sensitivity. *Chem. Eng. J.* **2015**, *268*: 60-66; https://doi.org/10.1016/j.cej.2015.01.024.
[20] He, G.S.; Yang, Z.J.; Pan, L.P.; Zhang, J.H.; Liu, S.J.; Yan, Q.L. Bioinspired Interfacial Reinforcement of Polymer-based Energetic Composites with a High Loading of Solid Explosive Crystals. *J. Mater. Chem. A*. **2017**, *26*: 13499-13510; https://doi.org/10.1039/c7ta03424e.
[21] Chen, L.; Li, Q.; Liu, S.S.; Bei, Y.Y.; Ding, Y.J.; Liu, J.; He, W.D. Bio-inspired Synthesis of Energetic Microcapsules Core-Shell Structured with Improved Thermal Stability and Reduced Sensitivity via In Situ Polymerization for Application Potential in Propellants. *Adv. Mater. Interfaces*, **2021**, *8*: paper 2101248; https://doi.org/10.1002/admi.202101248.
[22] He, G.S.; Li, X.; Bai, L.F.; Meng, L.; Dai, Y.; Sun, Y.S.; Zeng, C.C.; Yang, Z.J.; Yang, G.C. Multilevel Core-Shell Strategies for Improving Mechanical Properties of Energetic Polymeric Composites by the "Grafting-from" Route. *Compos. Part B*. **2020**, *191*: paper 107967; https://doi.org/10.1016/j.compositesb.2020.107967.
[23] Lin, C.M.; Gong, F.Y.; Qian, W.; Huang, X.N.; Tu, X.Q.; Sun, G.A.; Bai, L.F.; Wen, Y.S.; Yang, Z.J.; Li, J.; Guo, S.Y. Tunable Interfacial Interaction Intensity: Construction of a Bio-inspired Interface Between Polydopamine and Energetic Crystals. *Compos. Sci. Technol.* **2021**, *211*: paper 108816; https://doi.org/10.1016/j.compscitech.2021.108816.
[24] Liu, Y.L.; Ai, K.L.; Lu, L.H. Polydopamine and Its Derivative Materials: Synthesis and Promising Applications in Energy, Environmental, and Biomedical Fields. *Chem. Rev.* **2014**, *114*: 5067-5115; https://doi.org/10.1021/cr400407a.
[25] Zhu, Q.; Xiao, C.; Li, S.B.; Luo, G. Bioinspired Fabrication of Insensitive HMX Particles with Polydopamine Coating. *Propellants Explos. Pyrotech.* **2016**, *41*: 1092-1097; https://doi.org/10.1002/prep.201600021.
[26] Zhu, Q.; Wu, S.L.; Xiao, C.; Xie, X.; Li, S.B.; Luo, G. Bioinspired Improving Interfacial Performances of HMX, TATB and Aluminum Powders with Polydopamine Coating. *Chin. J. Energet. Mater.* **2019**, *27*: 949-954; https://doi.org/10.11943/CJEM2019179.
[27] Xiao, C.; Zhu, Q.; Xie, X.; Luo, G.; Li, S.B. Polydopamine Coated on Aluminum Powders and Its Disperse Stability in HTPB. *Chin. J. Explos. Propellants*, **2017**, *40*: 60-64; https://doi.org/10.14077/j.issn.1007-7812.2017.08.010.
[28] Duan, S.Y.; Wang, D.H.; Jiang, Q.P.; Xiao, C.; Liu, H.H.; Guo, Y.; Li, S.B.; Zhu, Q. Oxidant-Accelerated Polydopamine Modification Process for the Fast Fabrication of PDA on HMX with Improved Mechanical Stability. *Propellants Explos. Pyrotech.* **2021**, *46*: 751-757; https://doi.org/10.1002/prep.202000095.
[29] Yu, Q.; Zhao, C.D.; Zhu, Q.; Sui, H.L.; Yin, Y.; Li, J.S. Influence of Polydopamine

Coating on the Thermal Stability of 2,6-Diamino-3,5-dinitropyrazine-1-oxide Explosive Under Different Heating Conditions. *Thermochim. Acta* **2020**, *686*: paper 178530; https://doi.org/10.1016/j.tca.2020.178530.

[30] Jia, K.H.; Liu, Y.C.; Chai, T.; Yu, Y.W.; Jing, S.M.; Wu, P.F.; He, J.X.; Zhang, W. Fast Polymerization of Dopamine for Coating on ANPZO Surface with Excellent Thermal Stability and Mechanical Properties. *Propellants Explos. Pyrotech.* **2022**, *47*: paper e202100279; https://doi.org/10.1002/prep.202100279.

[31] Zeng, C.C.; Yang, Z.W.; Liu, J.H.; Ding, L.; Hao, S.L.; Gong, F.Y.; Yang, Z.J. Study on Mechanical Improvement of CL-20 Energetic Co-Crystals Based PBX by Surface Modification. *Propellants Explos. Pyrotech.* **2022**, *48*: paper e202200154; https://doi.org/10.1002/prep.202200154 .

[32] Daniel, W.W.; Paul, L.C.; Karl, S.H.; Colin, R.P. Controlling a Polymorphic Transition in 2,4-Dinitroanisole Using Crystal Doping. *Proc. New Trends Res. Energ. Mater.*, Pardubice, Czech Republic, **2015**.

[33] P'yanova, L.G.; Drozdov, V.A.; Sedanova, A.V.; Kornienko, N.V. An X-ray Photoelectron Spectroscopic Study of the Poly-N-vinylpyrrolidone Desorption from the Surface of a Granulated Carbon Sorbent. *Russ. J. Appl. Chem.* **2019**, *92*: 940-945; https://doi.org/10.1134/S1070427219070097.

[34] Abdul, G.L.; Mohammed, A. M.; Osama, S. On the Application of Two-dimensional Correlation Spectroscopy to Analyze X-ray Photoelectron Spectroscopic Data. *J. Polym. Res.* **2022**, *29*: 11; https://doi.org/10.1007/s10965-021-02857-8.

Received: October 7, 2023
Revised: June 27, 2024
First published online: June 28, 2024